Nanoscale

PAPER

View Article Online
View Journal | View Issue

Check for updates

Cite this: *Nanoscale*, 2023, **15**, 17544

Thin-film conformal fluorescent SU8-phenylenediamine†

Hani Barhum, *[a,b,c] Denis S. Kolchanov, [b,c] Mohammad Attrash,[d] Razan Unis,[a,e] Janis Alnis,[f] Toms Salgals,[g] Ibrahim Yehia[a] and Pavel Ginzburg[b,c]

The SU8 polymer is a negative photoresist widely used to produce high-quality coatings, with controllable thicknesses ranging from nanometers to millimeters, depending on fabrication protocols. Apart from conventional use cases in microelectronics and fluidics, SU8 is quite an attractive platform in nanophotonics. This material, being straightforwardly processed by ultraviolet lithography, is transparent to wavelengths longer than 500 nm. However, introducing fluorescent agents within the SU8 matrix remains a challenge owing to its high hydrophobicity. Here, we develop a process, where colorful quantum dots co-participate in the polymerization process by epoxide amination and become a part of a new fluorescent material – SU8-phenylenediamine. Through comprehensive characterization methods, including XPS and ^{1}H-NMR analyses, we demonstrate that *m*-PD covalently binds to SU8 epoxy sites with its molecular amine, virtually forming a new material and not just a mixture of two compounds. After characterizing the new strongly fluorescent platform, thin 300 nm films were created on several surfaces, including a conformal coverage of a nanofluidic capillary. This new process provides opportunities to incorporate various functional molecules into optoelectronic devices without the need for multistep deposition and surface functionalization.

Received 9th June 2023,
Accepted 2nd October 2023

DOI: 10.1039/d3nr02744a

rsc.li/nanoscale

Open Access Article. Published on 03 octobre 2023. Downloaded on 2026-06-01 19:15:44.
This article is licensed under a Creative Commons Attribution-NonCommercial 3.0 Unported Licence.

Introduction

The SU8 epoxy-based photoresist has gained significant attention since it was first introduced in 1995.[1] Since epoxy groups are crosslinked by being exposed to ultraviolet (UV) light (typically 365–405 nm) and form a stable solid structure, the polymer belongs to the family of negative photoresists.[2,3] After revealing numerous advantages of SU8, it became a technological platform across many disciplines, including microfluidics,[4–7] micromechanics,[8] biomedicine,[9] optoelectronics,[10,11] and many others.[12–15]

Superior mechanical and thermal stability along with great adhesion to a vast majority of commonly used surfaces (*e.g.*, glasses,[7] metals,[16] semiconductors,[17] and many others[18]) make SU8 a platform of choice in cases where facile low-cost fabrication of microstructures is required.[18,19] For example, structures with sharp edges and high aspect ratios approaching 1 : 20, 1 : 40, and even higher can be fabricated by photolithographic methods.[20] Furthermore, spin-coating protocols with accurately controlled parameters allow fabricating films with thicknesses ranging from sub-microns up to millimeters.[15]

Apart from its mechanical properties, SU8 is also an optically transparent material. Having a strong absorption in the UV range owing to benzene rings, the material is transparent for wavelengths longer than ~500 nm.[21,22] Due to its optical and mechanical properties, SU8 is employed for fabricating micro-fluidic channels, routinely used in various biological studies, *e.g.*, for cell culturing.[23] Three-dimensional SU8-based devices allow mimicking microenvironments experienced by cells in a complex tissue.[9,24] Incredible advances in the growth and differentiation of neural and muscle cells[25] encompass significant microfluidic components, where engineered thin-layer polymers play a role.[31] Microfluidic channels were developed to guide axonal development towards the muscle cells, paving the way for a deeper understanding of the pathology of amyotrophic lateral sclerosis (ALS).[26] Along with biological studies, many photonic applications have been explored.

[a]*Triangle Regional Research and Development Center, Kfar Qara' 3007500, Israel. E-mail: Hani.barhom@gmail.com*
[b]*Department of Electrical Engineering, Tel Aviv University, Ramat Aviv, Tel Aviv 69978, Israel*
[c]*Light-Matter Interaction Centre, Tel Aviv University, Tel Aviv, 69978, Israel*
[d]*Andrew and Erna Viterbi Department of Electrical Engineering, Technion, Haifa, Israel*
[e]*Department of Environmental Studies, Porter School of Environment and Earth Sciences, Tel Aviv University, Tel Aviv, Israel*
[f]*Institute of Atomic Physics and Spectroscopy, University of Latvia, Jelgavas Street 3, 1004 Riga, Latvia*
[g]*Institute of Telecommunications, Riga Technical University, 12 Azenes Street, 1048 Riga, Latvia*
† Electronic supplementary information (ESI) available. See DOI: https://doi.org/10.1039/d3nr02744a

This journal is © The Royal Society of Chemistry 2023

Open Access Article. Published on 03 octobre 2023. Downloaded on 2026-06-01 19:15:44.
This article is licensed under a Creative Commons Attribution-NonCommercial 3.0 Unported Licence.

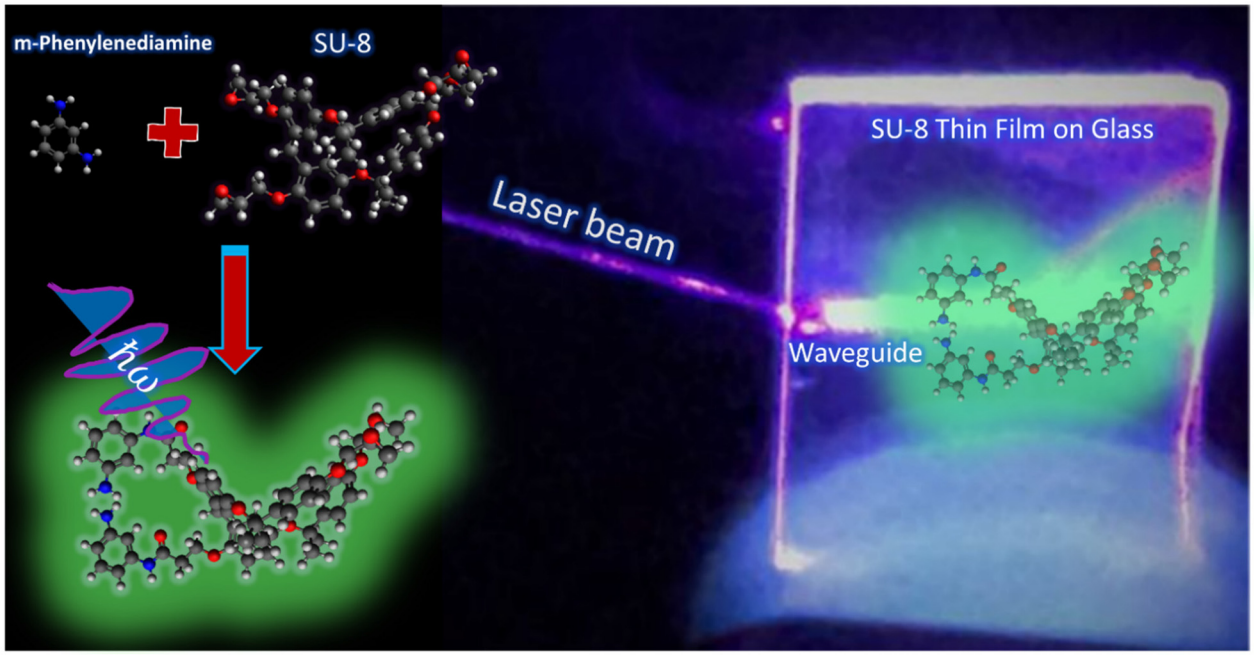

Fig. 1 Graphical illustrations and a practical application of the SU8 polymer before and after conjugation with *m*-phenylenediamine (*m*-PD). The upper left panel represents the dimeric form of the SU8 polymer prior to the conjugation process with *m*-PD. The lower left panel shows the resulting structure post-conjugation, depicting the modifications imparted to the SU8 polymer by *m*-PD. The right panel showcases a possible optoelectronic application: a glass slide with the polymer deposited onto its surface, and a waveguide fabricated within the polymer using a laser.

Waveguiding structures for sensing applications and integration within on-chip photonic circuits,[11,12] Mach–Zehnder SU8-based interferometers,[27,28] and on-chip microresonator-based biosensors with near-edge resonance[10,29] have been demonstrated to name just a few. Consequently, functionalized photonic and microfluidic SU8 technologies have emerged at the forefront of this rapidly evolving field, offering promising new possibilities and applications.

To endow SU8 with additional optical properties, structural functionalization with nanoparticles was demonstrated, introducing a range of plasmonic phenomena into light–matter interaction scenarios.[30] A direct linkage between molecular species and SU8 is quite appealing, and it is mainly done with the APTMS-GLut chemical binding to the surface enabling covalent attachment of desired molecules. The SU8's high hydrophobicity limits the interaction to the same kind of materials.[31] The low interaction forces with different materials along with the high chemical potential from the radical ester make its specific and labile bonding a nontrivial target. Since SU8 is widely used in biomedical studies, its functionalization is better to be performed with biocompatible fluorescent materials.[32–34] The biocompatibility of fluorescent agents is a significant area of its own, demanding the development of new platforms. Our focus is on phenylenediamine carbon dots, as we recently mastered their facile fabrication and sensing applications.[35] Specifically, a 90% reaction yield of carbon dots with a 70% quantum yield was demonstrated. As a result, matching those emitters with the low-cost SU8 polymer might have future technological benefits.

Here, we take advantage of the epoxy group in the SU8 polymer to spontaneously bind amine groups of phenylenediamine carbon dots. The covalent bonding of the molecules is integrated into the organic polymer skeleton, virtually forming a new material. This process makes the structure exhibit an inherently efficient fluorescence, which motivates the use of this new polymer in nanophotonics applications. To demonstrate the concept, we fabricated a series of devices by spin-coating thin films on flat coverslips and inner surfaces of micron-scale capillaries, which can be further designed for fluidic applications.

The manuscript is organized as follows: fabrication methods are presented first and then followed by an analysis and discussion on possible chemical reactions, responsible for the material formation. Then optical properties are presented of the bulk material with different aniline isomers. The characterization results are used for the structure analysis with molecular dynamic methods to predict the chemical composition and band gap. Fabrication of thin films and surface conjugation are discussed before the Conclusions section (Fig. 1).

Methods

Materials

Photoresists SU8-2000.5, -3005, and -3050, poly(ethylene glycol) methyl ether acrylate (PEGMEA) and the SU8 developer were purchased from Bachem (UK) Ltd, *meta*-phenylenediamine (*m*-PD), *ortho*-phenylenediamine (*o*-PD), *para*-

Open Access Article. Published on 03 octobre 2023. Downloaded on 2026-06-01 19:15:44.
This article is licensed under a Creative Commons Attribution-NonCommercial 3.0 Unported Licence.

phenylenediamine (*p*-PD), and hydrochloric acid (HCl) were purchased from Merck Ltd and 18 MΩ water.

SU8 conjugation to phenylenediamine

First, a solution of the desired phenylenediamine isomer (*para*, *ortho*, or *meta*, staying at a location on the amine group on the benzene ring[35]) is dissolved by sonication in the SU8 developer or in PEGMEA. The saturated solution is added in different amounts to 5 mL of polymer solution and mixed on a shaker. Visual inspection by observing the color of the product is done once the light yellow SU8 turned into a dark green solution (after 24 hours). Spectral changes occurred during mixing until stabilization and tracking was not quantified into kinetic data. HCl addition to the reaction mixture is done from a concentrated solution. All the concentrations are detailed in the Results and discussion section, where their impact on the resulting product is studied.

Film deposition and surface functionalization

Thin films were deposited on different substrates pre-cleaned with acetone and then rinsed with ethanol. After that, dried substrates are placed in a piranha solution until no bubbling appeared. Then samples were washed with DIW followed by EtOH and dried on a hot plate. *m*-PD saturated solution in hexane was prepared by vigorous mixing and sonication.

Functionalization was performed by sequentially immersing a freshly prepared, unpolymerized SU-8 film on a previously cleaned glass substrate with Piranha solution, and then dipping it in *m*-PD saturated solution in hexane for 5 minutes, followed by washing it in pure hexane for 1 min, and crosslinking the sample on a plate heated to 105 °C for 10 min.

Optical properties of conjugated SU8

Optical absorbance and fluorescence data were gathered using photoluminescence excitation (PLE) spectroscopy, carried out with a Synergy H1 plate reader. Absorbance spectra were obtained using a Macys1100 spectrophotometer, which featured a tungsten lamp source and a silicon photodiode detector. The instrument's spectral band was set at 2 nm, maintaining an accuracy of 1 nm. Prior to the tests, samples were diluted with deionized water. Fluorescence lifetime measurements were conducted using a PicoQuant system, employing a Taiko picosecond diode as a 375 nm excitation source. Lastly, confocal images were captured using the Leica 8 system.

ATR-Fourier transform infrared (FTIR) spectroscopy and proton nuclear magnetic resonance ^{1}H-NMR

The analysis was carried out using a Nicolet iS10 FTIR spectrometer equipped with a KBr/Ge beam splitter, optimized for the mid-infrared range, and a fast recovery deuterated triglycine sulfate (DTGS) detector. In this study, solid samples were analyzed in compliance with ASTM E1421 standards using the aforementioned spectrometer. The resultant FTIR data played an instrumental role in deciphering the molecular interactions between *m*-PD and SU8.

For the 1H-NMR analysis, dried and purified SU8-MPD powder was dissolved in chloroform and then introduced into a Bruker Ascend 500 high resolution NMR machine operating at a magnetic field of 500 MHz (11.7 Tesla). Spectra were obtained from both the SU8 and SU8-MPD samples after 48 hours of mixing.

Atomic force and scanning electron microscopy

Characterization of the film surface and cross-section thickness of the polymer film was performed using an environmental scanning electron microscope (ESEM). The surface roughness is further characterized using a JPLEC atomic force microscope (AFM).

Theoretical calculations

Theoretical calculations were performed using the CP2K code,[36] which uses a Gaussian basis set complemented by an auxiliary plane-wave basis set. Structures were drawn using the VESTA code.[37] We used a triple-ζ polarization quality Gaussian basis set (TZVP-MOLOPT-GTH)[38] and a 300 Ry plane-wave cutoff. The geometry optimization of the sample was performed using the Broyden–Fletcher–Goldfarb–Shanno (BFGS) routine by the Gaussian plane-wave (GPW) method with the combined density functional of B88 (exchange functional) and LYP,[39] where all atoms were relaxed until the residual force was smaller than 0.05 eV Å^{-1}. We applied a structural minimization algorithm using a non-periodic model in the Γ-point approximation. The electronic structure was investigated using the hybrid functional B3LYP.[40]

Results and discussion

Functionalizing SU8 polymers with fluorescent molecules presents distinct challenges. Typically, this process involves chemical binding at specific sites, facilitated by crosslinking molecules. However, changes in the dye's electronic structure during this process can potentially degrade their fluorescence. Notably, aggregate dye molecules may undergo concentration quenching effects, further impacting their fluorescence, *e.g.*, ref. 41. Therefore, refining the chemistry to achieve fluorescent polymers with high quantum yield becomes imperative.

Optical properties of SU8-phenylenediamine

Our exploration centers around the synthesis and optical properties of SU-8 polymers conjugated with phenylenediamine isomers, emphasizing the *meta* isomer (*m*-PD). Preliminary investigations distinguished *m*-PD for its superior fluorescence properties, exhibiting defined excitation and emission peaks and an enhanced emission intensity at increasing HCl concentrations. The ESI discusses the exhaustive comparative analyses involving *o*-PD and *p*-PD in detail (see Fig. S1†).

SU8 polymers display distinct absorbance properties based on their viscosity. For example, SU8-2000.5 reveals an increased absorbance at around 410 nm, with a pronounced peak observed at 0.65 M HCl (Fig. 2(a)). SU8-3005 and SU8-

 This journal is © The Royal Society of Chemistry 2023

Open Access Article. Published on 03 octobre 2023. Downloaded on 2026-06-01 19:15:44.
This article is licensed under a Creative Commons Attribution-NonCommercial 3.0 Unported Licence.

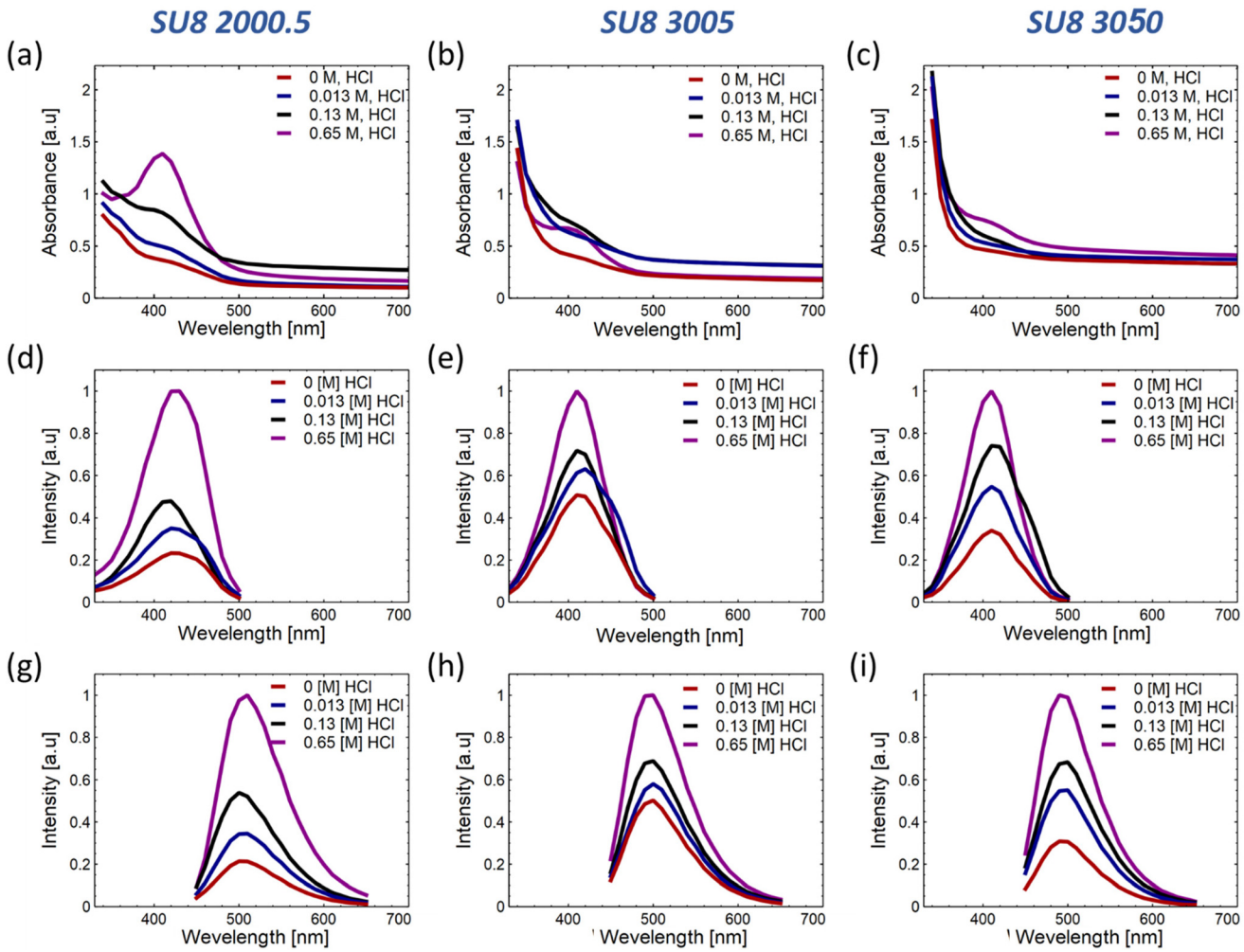

Fig. 2 Optical properties of SU8 polymers with varying viscosities (SU8-2000.5, SU-8-3005, and SU8-3050) conjugated with *m*-PD molecules and the influence of different amounts of hydrochloric acid being added to the reaction medium. The first column represents SU-8-2000.5, the second – SU8-3005, and the third – SU8-3050. (a–c) Absorbance spectra at 330 nm to 700 nm illustrate the impact of polymer viscosity. (d–f) PLE spectra (normalized) of the 530 nm emission peak, measured between 330 nm and 500 nm, highlighting the excitation-dependent behavior of the conjugates with varying viscosities. (g–i) Normalized emission spectra of conjugated SU-8 polymers at 450 and 650 nm range with excitation at 420 nm.

3050 exhibit similar absorption characteristics (Fig. 2(b and c)). A deeper insight into the corresponding PLE spectra is shown in Fig. 2(d–i) and the variations in emission intensities can be referred to in the ESI.†

To provide a comprehensive understanding of the optical modifications that emerge in the conjugated polymers, the characteristic peak values have been plotted against the proton concentration as shown in Fig. S2.† The identified trends imply that both the polymer's viscosity and the reaction medium's acidity exert a substantial influence on the conjugation efficiency and the enhancement of fluorescence properties.

It is hypothesized that polymers with a higher viscosity hinder the mobility of phenylenediamine molecules, consequently affecting the rate of conjugation and influencing the resulting absorbance and emission properties. Additionally, the acidity of the reaction medium can significantly impact the conjugation process. In this context, understanding the complex interactions between the polymer viscosity, the acidity of the reaction medium, and the conjugation efficiency becomes crucial for optimizing the optical properties of these innovative conjugated materials.

The collected data indicate that the absorbance of the conjugated SU8-2000.5 drops with the inclusion of HCl, while SU8-3005 and SU8-3050 seem to reach saturation at 0.65 M acid. This observation can likely be attributed to the medium's viscosity, which facilitates more substantial conjugation and intricate pathways, as suggested, and will be further elaborated using our hypothesized model in section 3.2. This insight also implies that comprehensive conjugation of *m*-PD molecules occurs at the polymer chains, leading to enhanced absorbance or extinction, as presented in Fig. S2(a).†

Interestingly, the SU8-2000.5 polymer displays a maximum PLE intensity in 0.13 M HCl, while the other polymers present

Open Access Article. Published on 03 octobre 2023. Downloaded on 2026-06-01 19:15:44.
This article is licensed under a Creative Commons Attribution-NonCommercial 3.0 Unported Licence.

a gradual increase that moderates at higher concentrations, as illustrated in Fig. S2(b).† The relatively lower viscosity and polymer concentration of SU8-2000.5 refer to the formation of more conjugation and bonds between the *m*-PD and the polymer, as well as among polymer chains. However, this process could also create additional bonds that do not contribute to fluorescence and might even interfere with some fluorescent sites. As observed in Fig. S2(b and c),† the rise in fluorescence intensity for SU8-3005 and SU8-3050, alongside the decrease in intensity for SU8-2000.5, which allows assuming that the bonds formed in the initial stages of the reaction contribute more significantly to the formation of fluorescent species, while the later-formed bonds do not have the same impact. Furthermore, when the concentration of acid outstrips the availability of epoxy sites, the rate of formation of non-contributing bonds increases, thereby potentially disrupting the fluorescent conjugated spots.

After observing the macroscopic optical properties of SU8-*m*-PD, the molecular mechanisms of the material formation will be explored.

Molecular conjugations to phenylenediamine

The synthesis of *m*-PD conjugated with SU8 epoxy begins with the reaction between the amine group of *m*-PD and epoxy groups of SU8, resulting in the formation of secondary amines and the opening of epoxy rings. The reaction continues, leading predominantly to the formation of tertiary amines. This forms our starting point of investigation. It's important to acknowledge that this model, while informed by DFT modeling and an array of collected experimental data, is postulated based on current understanding and findings. It is built on extensive literature about amine to epoxy reactions and supported by our DFT calculations, but it is still, inherently, a proposition open for further investigation and refinement. Apart from fluorescence studies, FTIR spectra were required to shed light on the complex reaction. The spectrum evolution by adding *m*-PD at different concentrations offers insights into the chemical transformation occurring during this synthesis as shown in Fig. 3.

In Fig. 3(a), the spectrum of pure SU8 displayed peaks representative of different bonds within the polymer. The aromatic ring-related C–C stretching[42–47] vibrations were revealed through peaks at 559.60 cm^{-1}, 658.42 cm^{-1}, and 754.18 cm^{-1}. The peak at 910.23 cm^{-1} indicated the presence of epoxy groups due to the characteristic C–O stretching vibrations. With the addition of *m*-PD to SU8, the spectra showed noticeable changes as seen in Fig. 3(b and c). A new peak emerged at 1055.43 cm^{-1}, which might indicate C–N stretching vibrations, potentially confirming the formation of secondary amine bonds.

Further addition of *m*-PD resulted in a continued decrease in intensities of epoxy-associated peaks, as shown in Fig. 3(d). Concurrently, there was an increase in the intensity of peaks around 3680.24 cm^{-1} and 3705.38 cm^{-1}, hinting at the conversion of epoxy groups to free hydroxyl groups. It is also worth noting that secondary amine formation might be debatable, as FTIR peaks might shift and smear.

As shown in Fig. 3(e), the primary product of the reaction appears to be tertiary aromatic amines. Interestingly, there was a lack of N–H stretching peaks in the range of 3400–3200 cm^{-1}, leading us to believe that all of the *m*-PD is used up during the reaction, without the significant formation of primary or secondary amines.

There was, however, debate around the existence of primary and secondary amines. Some suggested that terminal groups could remain as primary or secondary amines, despite the absence of clear evidence in the FTIR data. Also, the possibility of hidden peaks under the dominant signals around 3000 and 3600 cm^{-1} was raised. A different perspective on the formation of N–N or N–O bonds was also presented. Although the FTIR spectra didn't show clear evidence, the theoretical feasibility was suggested through DFT calculations.

Building upon the data presented in Fig. 3 from the FTIR spectrum, we turn to the ^{1}H-NMR spectrum in Fig. 4 to further probe the interaction between *m*-PD and SU8 epoxy. In Fig. 4(a), the overall ^{1}H-NMR spectrum provides a foundational reference, setting the stage for more detailed analysis. Fig. 4(b), focusing on the region from 0 to 2.25 ppm, predominantly captures the resonances of aliphatic protons inherent to the SU8 structure. This suggests that the core structure of SU8 remains unaffected mainly after the conjugation process. Transitioning to Fig. 4(c), which encompasses the 2.25–4.5 ppm region, we observe potential indications of the secondary or tertiary amine structures. The integration values within this region align with our previous observations from the FTIR study, hinting at the formation of secondary amines and possibly the evolution to tertiary amines. Lastly, in Fig. 4(d), ranging from 6.5 to 8 ppm, the aromatic proton signals come to the forefront. A notable shift in integration values from the sole SU8 to the *m*-PD conjugated SU8 provides indirect evidence of *m*-PD's aromatic protons finding their place within the new structural framework. This shift reaffirms that *m*-PD has successfully interacted with SU8 epoxy.

The data from the ^{1}H-NMR spectrum in Fig. 4 lends further credence to our proposed reaction mechanism and complements our FTIR findings. The subtle yet discernible changes across different regions of the spectrum paint a coherent picture of the chemical transformation underway.

X-ray photoelectron spectroscopy (XPS) provides detailed insights into the surface atomic composition of materials. Analyzing Fig. S3(a–c)† for pure SU8 and Fig. S3(d–f)† for SU8-*m*PD, distinct elemental variations emerge that substantiate the integration of *m*-PD into the SU8 matrix.

Table S1† elucidates the atomic percentages for the SU8 sample, highlighting prominent peaks for carbon (C 1s, 71.93%) and oxygen (O 1s, 22.44%). Upon conjugation to *m*-PD, as presented in Table S2,† the carbon content slightly elevates to 73.01%, while the oxygen experiences a marginal decrement to 21.90%. However, the defining evidence is the emergence of the N 1s peak at 1.22%, absent in the pure SU8 sample.

 This journal is © The Royal Society of Chemistry 2023

Open Access Article. Published on 03 octobre 2023. Downloaded on 2026-06-01 19:15:44.
This article is licensed under a Creative Commons Attribution-NonCommercial 3.0 Unported Licence.

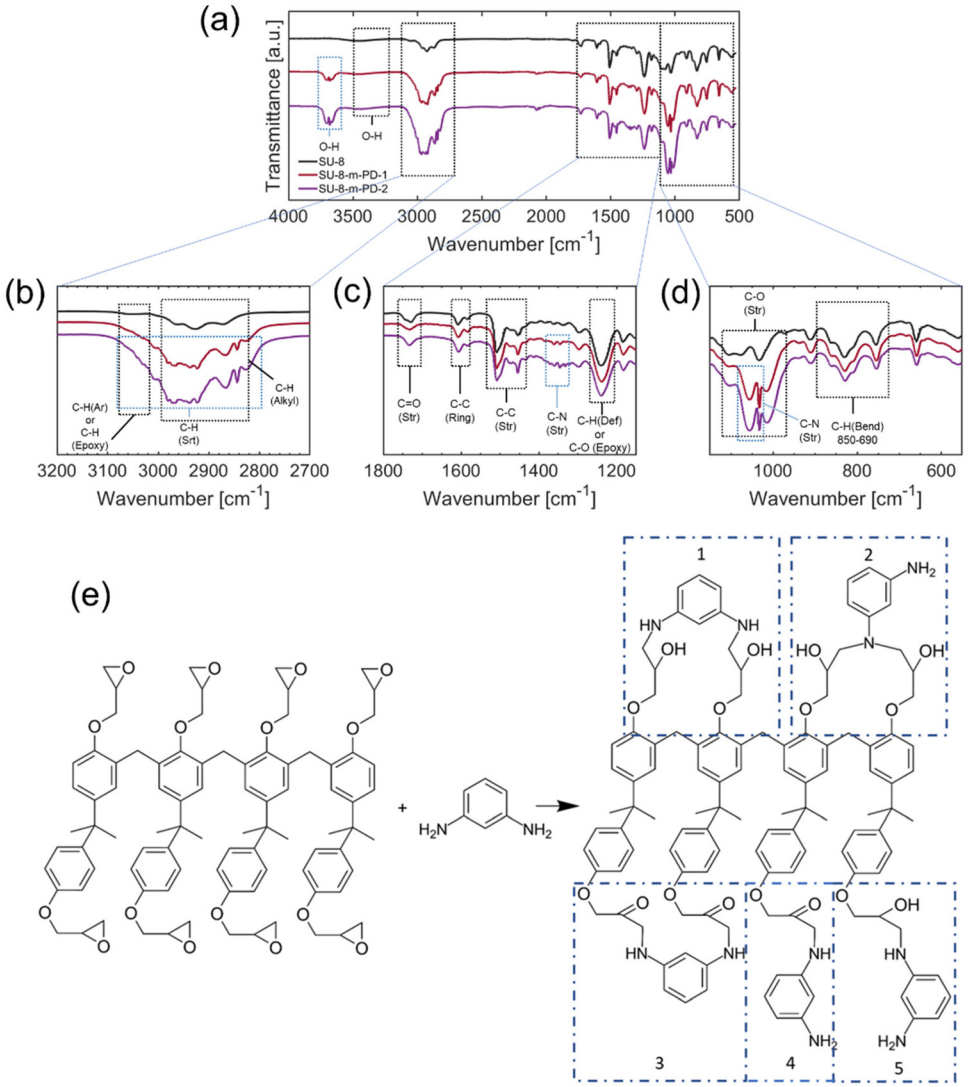

Fig. 3 (a) Full-range ATR Fourier-transform infrared (FTIR) spectra of the conjugation process between *meta*-phenylenediamine (*m*-PD) and SU8, indicating the characteristic peaks corresponding to the functional groups involved. This spectrum provides an overview of the complex interactions that transpire during the conjugation process. (b) Detailed FTIR spectra in the 2800–3100 cm^{-1} region, highlighting the specific vibrations attributed to various functional groups. (c) FTIR spectra in the 1150–1800 cm^{-1} region, further delineating the presence of different functional group vibrations, including the potential formation of secondary amine and amide bonds. (d) FTIR spectra in the 1150–550 cm^{-1} region, emphasizing the broad range of potential functional group interactions. The distinct peaks in this region are instrumental in deducing the nature of the interactions. (e) Several structures among the proposed configurations, while other options are analyzed further and hypothesized as less probable, and (except for model 2) the others are in the first stage toward tertiary amination.

Mathematically, let the content of *m*-PD in the SU8-*m*PD composite be represented by p. Based on the atomic ratios derived from the XPS data and the structure of *m*-PD, we estimate:

$$p \approx \frac{1.22\%\,(\mathrm{N}\,1s)}{6(\mathrm{C\ atoms}) + 2(\mathrm{N\ atoms})} \quad (1)$$

From this equation, we deduce that the *m*-PD content in the SU8-*m*PD composite ranges between 4.88% and 9.95%. This gives us an *m*-PD : SU8 monomer ratio ranging from 1 : 19.5 to 1 : 10.05. These XPS findings, evident from Tables S1 and S2,† consistently align with the transformations observed in Fig. 3 from the FTIR analysis and the variances in aromatic and aliphatic regions seen from the ^{1}H-NMR spectrum in Fig. 4. Collectively, these results form a cohesive narrative, reinforcing the hypothesis of the successful conjugation of *m*-PD to the SU8 structure. Moreover, the XPS data extend our understanding by offering quantitative insight into this conjugation, strengthening the foundation for further explorations into modified SU8 systems.

DFT calculations

The *m*-PD and SU8 reaction is hypothesized relying on DFT calculations and available experimental data. A range of plausible molecular configurations will be proposed next, offering a

Open Access Article. Published on 03 octobre 2023. Downloaded on 2026-06-01 19:15:44.
This article is licensed under a Creative Commons Attribution-NonCommercial 3.0 Unported Licence.

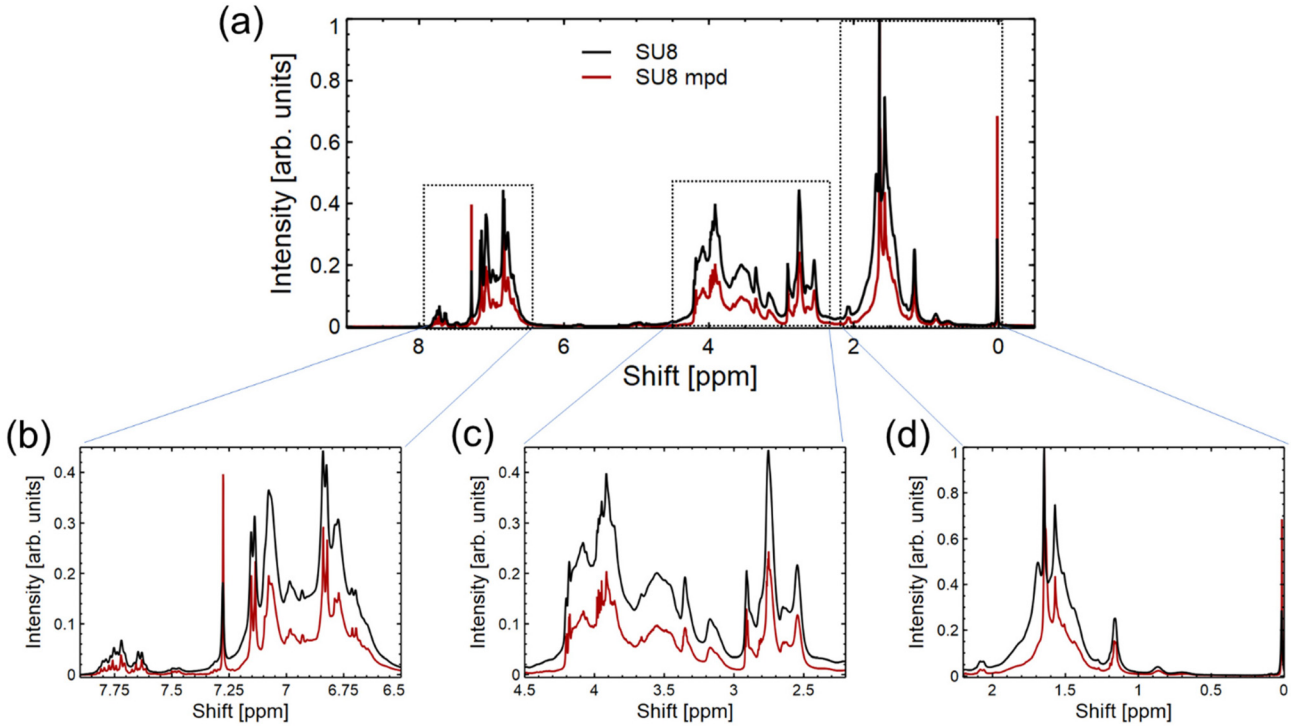

Fig. 4 ^{1}H-NMR analysis of the SU8-*m*PD conjugate. (a) Provides a full view of the entire spectrum. Region-specific magnifications further elucidate the interactions: (b) emphasizing the 6.5–8 ppm range, which is dominated by aromatic proton resonances, indicative of the SU8 and *m*-PD aromatic structures. (c) The 2.25–4.5 ppm region, highlighting potential transitional groups and intermediates; and (d) focusing on the 0–2.25 ppm range, predominantly showcasing aliphatic proton environments.

unique perspective on how *m*-PD and SU8 interact, as illustrated in Fig. 5(a–d).

Starting with Fig. 5(a), tertiary amine formation is shown, which involves an *m*-PD molecule and an SU8 monomer. Here, the *m*-PD molecule forms bonds with two epoxy groups of the SU8 monomer, leading to a tertiary amine configuration. This is in line with the well-established behavior of amines reacting with epoxy groups. Furthermore, the calculated band gap for this configuration, 4.4 eV does not fall within the range of the observed green light emission in our absorption and emission spectra. Fig. 5(b) presents an alternative configuration where one *m*-PD molecule bridges two SU8 monomers by forming two amide bonds. The calculated band gap for this structure is 3.6 eV, which aligns with the energy range corresponding to green fluorescence. This configuration supports the FTIR spectra, where a new peak at 1080 cm^{-1}, indicative of C–N stretching vibrations associated with amide bonds, is evident. Fig. 5(c) shows another possible configuration, this time featuring the formation of nitro (N–O) groups. In this scenario, one amine group from the *m*-PD molecule forms an amide bond with the SU8 monomer, while the other amine group creates an N–O bond. The band gap for this structure is calculated to be 3.6 eV, which fits well within the energy requirements for green light emission. Yet, this structure is not fully supported by FTIR. Lastly, Fig. 5(d) shows a complex scenario involving *m*-PD dimerization *via* N–N bond formation. The resulting dimer interacts with SU8 epoxy groups, leading to the formation of amide bonds. Despite the theoretically calculated band gap of 2.6 eV being compatible with green fluorescence, the FTIR spectra do not provide explicit indications of N–N bond formation, suggesting that this configuration may not substantially contribute to the overall characteristics of the *m*-PD-SU8 composite.

Our DFT calculations and corresponding experimental data suggest that tertiary amine formation involving two epoxy groups is the most probable outcome of the *m*-PD-SU8 interaction, as shown in Fig. 3(e). Other plausible configurations, such as those involving secondary amines, amide bonds, and potentially N–N and N–O bonds, may also exist but likely contribute less significantly to the overall properties of the synthesized material. For a more comprehensive analysis of possible molecular structures, see Fig. S4† and discussion.

Thin film deposition and surface functionalization

Owing to the well-established adhesive properties of SU8 on a wide range of surfaces, it is crucial to evaluate the performance of our newly developed fluorescent derivative when forming thin film deposition on BK7 glass and indium tin oxide (ITO) coated glass. These substrates were chosen due to their common usage in optical and electronic applications, respectively. To explore the adhesion and film formation of SU8-*m*-PD, we prepared thin films of each material using the spin coating method. Consistent parameters were maintained to ensure comparability. The spin-coating process was conducted

 This journal is © The Royal Society of Chemistry 2023

Open Access Article. Published on 03 octobre 2023. Downloaded on 2026-06-01 19:15:44.
This article is licensed under a Creative Commons Attribution-NonCommercial 3.0 Unported Licence.

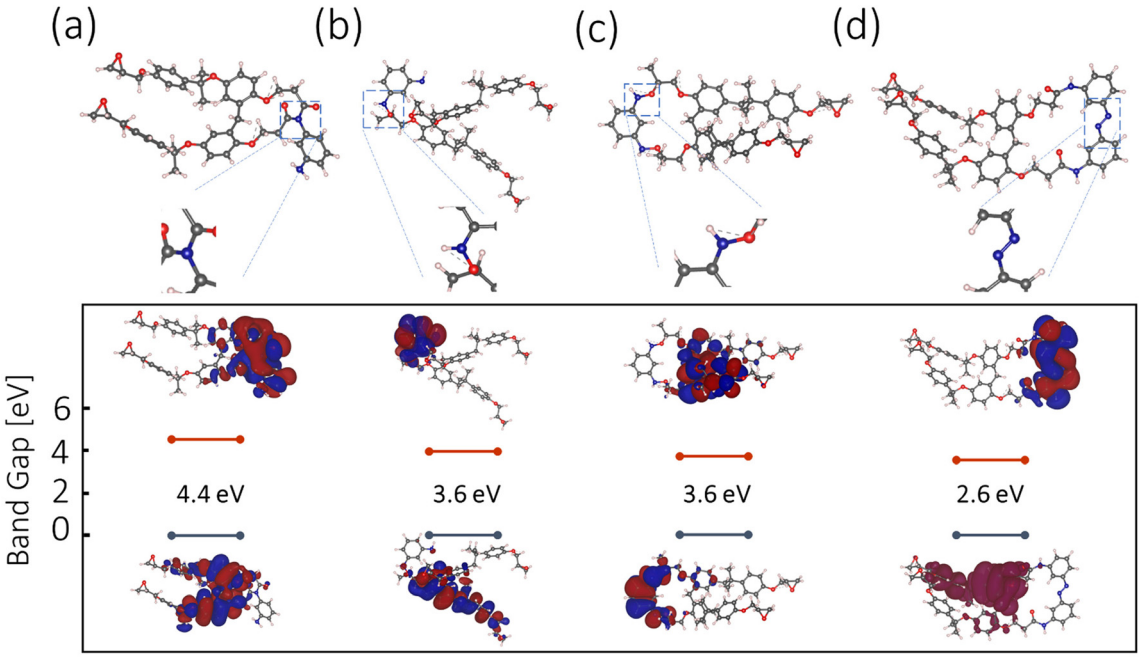

Fig. 5 (a–d) Probable molecular structures of the *m*-PD-SU8 composite. The structures visualize the possible conformations resulting from the interaction between *m*-PD molecules and SU8 polymers. Each structure is presented as (a), (b), (c) and (d), demonstrating different plausible formations with band gap energies suitable for green emission. These structures were visualized and rendered using the VESTA software. Alongside each molecular structure, the calculated band gaps are provided, accompanied by the respective highest occupied molecular orbital (HOMO, shown at the bottom) and the lowest unoccupied molecular orbital (LUMO, shown at the top) charge distributions.

at speeds of 2k, 3k, and 4k rpm. Importantly, we found that the film thickness is identical to what appears in the SU8 2000.5 datasheet.

The cross-sections of the SU8-*m*-PD conjugate thin films deposited on glass substrates are depicted in the HRSEM images in Fig. 6. Specifically, Fig. 6(b) showcases a cross-section captured in backscatter mode, revealing a consistent thickness of about 300 nm. Fig. 6(a), captured in normal mode, illustrates the uniformity of the film structure, with its inset providing a closer look at a specific area at higher magnification. These images attest to the effectiveness of the spin-coating process executed at 6000 rpm.

Fig. 6(c) shows an Atomic Force Microscopy (AFM) topographical depiction of a compact 5 × 5 μm area of the SU8-*m*-PD thin film. The image effectively demonstrates the film's minimal surface roughness and superb uniformity, both critical attributes for enhancing the device performance. The confocal microscopy images presented in Fig. 6(d) offer a comprehensive perspective on the fluorescence profiles of the SU8-*m*-PD conjugate films in three Cartesian planes (XY, XZ, and YZ). The uniform distribution of fluorescence throughout the film shows the effectiveness of the *m*-PD conjugation process, which has potentially broad applications in bioimaging. For instance, the film could serve as a contrast agent in fluorescence microscopy or as a biomarker in cellular imaging, offering enhanced visualization of biological samples.

In the ESI, Fig. S4† provides a deeper insight into the surface features of the *m*-PD-SU8 thin film. The Atomic Force

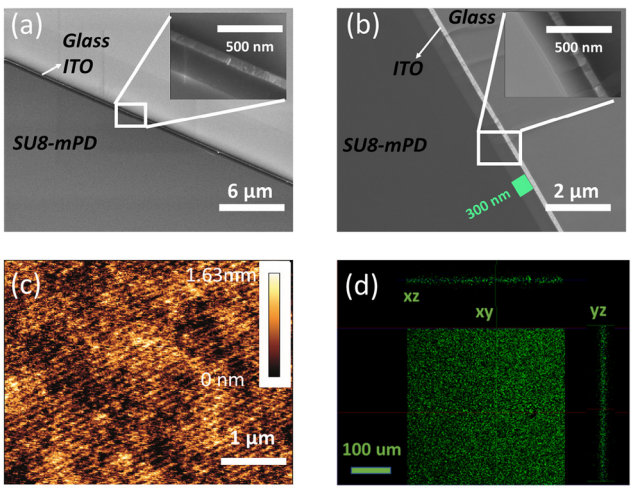

Fig. 6 Characterization of the SU8-*m*-PD conjugated thin films. (a) HRSEM image of the *m*-PD conjugated film in normal mode, showcasing the adherence and consistency of the film with an inset displaying an enlarged view of a marked area at higher magnification. (b) HRSEM image of a cross-section of the *m*-PD conjugated film on a substrate, captured in backscatter mode, illustrating the film's thickness and uniformity, with an inset providing a magnified perspective of a designated region. (c) High-resolution AFM image of a 5 × 5 μm area of the *m*-PD-SU8 film, demonstrating minimal surface roughness and high uniformity. (d) Confocal images in XY, XZ, and YZ planes of the *m*-PD film deposited on a glass substrate under 488 nm excitation, presenting the film's fluorescence profiles and spatial distribution.

Open Access Article. Published on 03 octobre 2023. Downloaded on 2026-06-01 19:15:44.
This article is licensed under a Creative Commons Attribution-NonCommercial 3.0 Unported Licence.

Microscopy (AFM) topographical images clearly illustrate the film's exceptional surface uniformity and near-negligible roughness. This uniformity and smoothness are crucial properties, especially considering the intended optoelectronic applications where surface irregularities could compromise the performance of the devices. Fig. S6† illustrates the potential of our synthesized *m*-PD-SU8 composite. In part (a), a Scanning Electron Microscopy (SEM) image that shows the composite's conformality as it impeccably coats a capillary fiber, attesting to its potential in applications demanding intricate conformal coatings such as in optoelectronics and biocompatible devices. Fig. S6(b)† shows an optical fluorescence image that reveals the capillary with green SU8 emission under UV excitation, highlighting the composite's promising prospects in fluorescence-based applications, including optical sensors and imaging systems. The demonstrated integration of the *m*-PD-SU8 composite into a fiber optic context thus underscores its promise in advanced photonic devices.

Conclusions

In our detailed study, we employed a series of analytical techniques to understand the synthesis and properties of SU8 polymers conjugated with phenylenediamine isomers, emphasizing *meta*-phenylenediamine (*m*-PD). Optical spectroscopy highlighted distinct optical behaviors of the conjugated polymers, with well-defined excitation and emission peaks. The FTIR spectra confirmed the presence of molecular bonding associated with conjugation, complemented by shifts in the ^{1}H NMR data, which indicated molecular modifications in the synthesized material. XPS analyses further showcased specific chemical functionalities in line with the proposed synthetic route. Furthermore, the estimated value of *m*-PD conjugates per SU8 monomer based on XPS elemental analysis was performed, suggesting more insights into the polymer functionality and ability for microlithography. While the results are promising, we remain conscious that the models presented are interpretations based on current data. Factors such as HCl concentration and polymer viscosity were methodically examined, and their influences on the optical properties of the conjugates were elucidated. ESEM and confocal microscopy visuals provided additional insights into the uniformity and consistency of the deposited materials on various substrates, from flat films to contoured capillaries.

The approach of epoxy-amine conjugation, as outlined, suggests its potential in pioneering the development of polymers with unique optical and mechanical properties. Guided by these findings, this study hopes to contribute constructively to further research in surface-functionalized polymers and their potential applications.

Author contributions

Hani Barhum: investigation, formal analysis, methodology, writing – original draft, and writing – review & editing. Dennis Kolchanov: investigation and formal analysis. Mohammad Attrash: investigation, formal analysis, and DFT. Razan Unis: investigation and formal analysis. Janis Alnis: investigation and formal analysis. Toms Salgals: investigation and formal analysis. Ibrahim Yehia: investigation and formal analysis. Pavel Ginzburg: conceptualization, writing – review & editing, and supervision.

Conflicts of interest

There are no conflicts to declare.

Acknowledgements

This research was funded by the ERC StG "In Motion" (802279), PAZY Foundation (Grant No. 01021248), Tel Aviv University Breakthrough Innovative Research Grant, the Ministry of Science, Technology and Space of Israel (Grant No. 79518), and also European Regional Development Fund project 1.1.1.5/19/A/003. We wish to thank Professor Joan Adler for the access to computational resources in the facility.

References

1 N. C. LaBianca and J. D. Gelorme, High-Aspect-Ratio Resist for Thick-Film Applications, in *Advances in Resist Technology and Processing XII*, 1995, vol. 2438, DOI: 10.1117/12.210413.
2 J. M. Shaw, J. D. Gelorme, N. C. LaBianca, W. E. Conley and S. J. Holmes, Negative Photoresists for Optical Lithography, *IBM J. Res. Dev.*, 1997, **41**(1–2), 81–94, DOI: 10.1147/rd.411.0081.
3 R. Feng and R. J. Farris, Influence of Processing Conditions on the Thermal and Mechanical Properties of SU8 Negative Photoresist Coatings, *J. Micromech. Microeng.*, 2003, **13**(1), 80–88, DOI: 10.1088/0960-1317/13/1/312.
4 C. H. Lin, G. B. Lee, B. W. Chang and G. L. Chang, A New Fabrication Process for Ultra-Thick Microfluidic Microstructures Utilizing SU-8 Photoresist, *J. Micromech. Microeng.*, 2002, **12**(5), 590–597, DOI: 10.1088/0960-1317/12/5/312.
5 F. S. Hamdi, M. Woytasik, M. Couty, O. Francais, B. Le Pioufle and E. Dufour-Gergam, Low Temperature Irreversible Poly(DiMethyl) Siloxane Packaging of Silanized SU8 Microchannels: Characterization and Lab-on-Chip Application, *J. Microelectromech. Syst.*, 2014, **23**(5), 1015–1024, DOI: 10.1109/JMEMS.2014.2331454.
6 M. Talebi, P. Woias and K. Cobry, Analysis of Impedance Data from Microfluidic Device with on-Channel Sensors, *Sens. Actuators, A*, 2018, **279**, 543–552, DOI: 10.1016/j.sna.2018.07.004.
7 M. Talebi, K. Cobry, A. Sengupta and P. Woias, *Transparent Glass/SU8-Based Microfluidic Device with on-Channel Electrical Sensors*, 2017. DOI: 10.3390/proceedings1040336.

This journal is © The Royal Society of Chemistry 2023

Open Access Article. Published on 03 octobre 2023. Downloaded on 2026-06-01 19:15:44.
This article is licensed under a Creative Commons Attribution-NonCommercial 3.0 Unported Licence.

8 B. Krishna, A. Chaturvedi, N. Mishra and K. Das, Nanomechanical Characterization of SU8/ZnO Nanocomposite Films for Applications in Energy-Harvesting Microsystems, *J. Micromech. Microeng.*, 2018, **28**(11), 115013, DOI: 10.1088/1361-6439/aae10c.

9 J. H. T. Ransley, M. Watari, D. Sukumaran, R. A. McKendry and A. A. Seshia, SU8 Bio-Chemical Sensor Microarrays, *Microelectron. Eng.*, 2006, **83**(4–9 SPEC. ISS.), 1621–1625, DOI: 10.1016/j.mee.2006.01.175.

10 B. Bêche, E. Gaviot, C. Godet, A. Zebda, A. Potel, J. Barbe, L. Camberlein, V. Vié, P. Panizza, G. Loas, C. Hamel, J. Zyss and N. Huby, Spin Coating and Plasma Process for 2.5D and Hybrid 3D Micro-Resonators on Multilayer Polymers, in *Optical Sensors*, 2009, **7356**, 70–79, DOI: 10.1117/12.820339.

11 B. Bêche, Integrated Photonics Devices on SU8 Organic Materials, *Int. J. Phys. Sci.*, 2010, **5**(5), 612–618.

12 R. Müller, D. Cristea, M. Kusko, P. Obreja, D. Esinenco, V. Damian and P. C. Logofatu, SU8 Polymer Materials Used in Integrated Optic Microsystems, *Optoelectron. Adv. Mater., Rapid Commun.*, 2010, **4**(2), 228–233.

13 B. Gorissen, C. Van Hoof, D. Reynaerts and M. De Volder, SU8 Etch Mask for Patterning PDMS and Its Application to Flexible Fluidic Microactuators, *Microsyst. Nanoeng.*, 2016, **2**, 1–5, DOI: 10.1038/micronano.2016.45.

14 S. Yardi, A. Gupta, P. Sundriyal, G. Bhatt, R. Kant, D. Boolchandani and S. Bhattacharya, High Efficiency Coupling of Optical Fibres with SU8 Micro-Droplet Using Laser Welding Process, *Lasers Manuf. Mater. Process.*, 2016, **3**(3), 147–157, DOI: 10.1007/s40516-016-0027-6.

15 Y. Tian, X. Shang, Y. Wang and M. J. Lancaster, Investigation of SU8 as a Structural Material for Fabricating Passive Millimeter-Wave and Terahertz Components, *J. Micro/Nanolithogr., MEMS, MOEMS*, 2015, **14**(4), 044507, DOI: 10.1117/1.jmm.14.4.044507.

16 B. F. E. Matarèse, P. L. C. Feyen, A. Falco, F. Benfenati, P. Lugli and J. C. Demello, Use of SU8 as a Stable and Biocompatible Adhesion Layer for Gold Bioelectrodes, *Sci. Rep.*, 2018, **8**(1), DOI: 10.1038/s41598-018-21755-6.

17 J. Wan, S. R. Deng, R. Yang, Z. Shu, B. R. Lu, S. Q. Xie, Y. Chen, E. Huq, R. Liu and X. P. Qu, Silicon Nanowire Sensor for Gas Detection Fabricated by Nanoimprint on SU8/SiO_2/PMMA Trilayer, *Microelectron. Eng.*, 2009, **86**(4–6), 1238–1242, DOI: 10.1016/j.mee.2008.12.022.

18 S. Charlot, A. M. Gué, J. Tasselli, A. Marty, P. Abgrall and D. Estève, A Low Cost and Hybrid Technology for Integrating Silicon Sensors or Actuators in Polymer Microfluidic Systems, *J. Micromech. Microeng.*, 2008, **18**(1), DOI: 10.1088/0960-1317/18/1/017003.

19 H. Lorenz, M. Despont, N. Fahrni, N. LaBianca, P. Renaud and P. Vettiger, SU-8: A Low-Cost Negative Resist for MEMS, *J. Micromech. Microeng.*, 1997, **7**(3), 121–124, DOI: 10.1088/0960-1317/7/3/010.

20 M. McNie, D. King, C. Vizard, A. Holmes and K. W. Lee, High Aspect Ratio Micromachining (HARM) Technologies for Microinertial Devices, *Microsyst. Technol.*, 2000, **6**(5), 184–188, DOI: 10.1007/s005420000044.

21 J. Rajendran, S. Sathiamoorthy, K. J. Tiwari, T. S. Suraj, M. S. Ramachandra Rao and P. Malar, Growth of Antimony Selenide Solar Absorber on Micro Textured Substrates for Efficient Light Trapping and Enhanced Optical Absorption, *Sol. Energy*, 2020, **211**, 977–987, DOI: 10.1016/j.solener.2020.10.030.

22 J. C. Ramirez, J. N. Schianti, M. G. Almeida, A. Pavani, R. R. Panepucci, H. E. Hernandez-Figueroa and L. H. Gabrielli, Low-Loss Modified SU-8 Waveguides by Direct Laser Writing at 405 Nm, *Opt. Mater. Express*, 2017, **7**(7), 2651–2659, DOI: 10.1364/ome.7.002651.

23 R. Maimon and E. Perlson, Muscle Secretion of Toxic Factors, Regulated by MiR126-5p, Facilitates Motor Neuron Degeneration in Amyotrophic Lateral Sclerosis, *Neural Regener. Res.*, 2019, **14**(6), 969–970, DOI: 10.4103/1673-5374.250571.

24 J. W. Kamande, Y. Wang and A. M. Taylor, Cloning SU8 Silicon Masters Using Epoxy Resins to Increase Feature Replicability and Production for Cell Culture Devices, *Biomicrofluidics*, 2015, **9**(3), DOI: 10.1063/1.4922962.

25 S. H. Choi, Y. H. Kim, M. Hebisch, C. Sliwinski, S. Lee, C. D'Avanzo, H. Chen, B. Hooli, C. Asselin, J. Muffat, J. B. Klee, C. Zhang, B. J. Wainger, M. Peitz, D. M. Kovacs, C. J. Woolf, S. L. Wagner, R. E. Tanzi and D. Y. Kim, A Three-Dimensional Human Neural Cell Culture Model of Alzheimer's Disease, *Nature*, 2014, **515**(7526), 274–278, DOI: 10.1038/nature13800.

26 T. Altman, A. Ionescu, A. Ibraheem, D. Priesmann, T. Gradus-Pery, L. Farberov, G. Alexandra, N. Shelestovich, R. Dafinca, N. Shomron, F. Rage, K. Talbot, M. E. Ward, A. Dori, M. Krüger and E. Perlson, Axonal TDP-43 Condensates Drive Neuromuscular Junction Disruption through Inhibition of Local Synthesis of Nuclear Encoded Mitochondrial Proteins, *Nat. Commun.*, 2021, **12**, 1–17, DOI: 10.1038/s41467-021-27221-8.

27 N. Pelletier, B. Bêche, N. Tahani, J. Zyss, L. Camberlein and E. Gaviot, SU-8 Waveguiding Interferometric Micro-Sensor for Gage Pressure Measurement, *Sens. Actuators, A*, 2007, **135**(1), 179–184, DOI: 10.1016/j.sna.2006.07.012.

28 N. Pelletier, B. Bêche, E. Gaviot, L. Camberlein, N. Grossard, F. Polet and J. Zyss, Single-Mode Rib Optical Waveguides on SOG/SU-8 Polymer and Integrated Mach-Zehnder for Designing Thermal Sensors, *IEEE Sens. J.*, 2006, **6**(3), 565–570, DOI: 10.1109/JSEN.2006.874489.

29 A. Zebda, L. Camberlein, B. Bêche, E. Gaviot, E. Bêche, D. Duval, J. Zyss, G. Jézéquel, F. Solal and C. Godet, Spin Coating and Plasma Process for 2.5D Integrated Photonics on Multilayer Polymers, *Thin Solid Films*, 2008, **516**(23), 8668–8674, DOI: 10.1016/j.tsf.2008.04.095.

30 A. Falco, B. Matarese, P. Feyen, F. Benfenati, P. Lugli and J. C. De Mello, Investigation, of the Stability and Biocompatibility of Commonly Used Electrode Materials in Organic Neurooptoelectronics, *IEEE Trans. Nanotechnol.*, 2016, **15**(5), 746–753, DOI: 10.1109/TNANO.2016.2536946.

31 J. Li, Y. Zhao, M. Ge, S. Fu and T. Lin, Superhydrophobic and Luminescent Cotton Fabrics Prepared by Dip-Coating

Open Access Article. Published on 03 octobre 2023. Downloaded on 2026-06-01 19:15:44.
This article is licensed under a Creative Commons Attribution-NonCommercial 3.0 Unported Licence.

of APTMS Modified SrAl2O4:Eu2+,Dy3+ Particles in the Presence of SU8 and Fluorinated Alkyl Silane, *J. Rare Earths*, 2016, **34**(7), 653–660, DOI: **10.1016/S1002-0721(16)60075-3**.

32 B. Apter, N. Lapshina, H. Barhom, B. Fainberg, A. Handelman, A. Accardo, C. Diaferia, P. Ginzburg, G. Morelli and G. Rosenman, Fluorescence Phenomena in Amyloid and Amyloidogenic Bionanostructures, *Crystals*, 2020, **10**(8), 1–43, DOI: **10.3390/cryst10080668**.

33 H. Bahrom, A. A. Goncharenko, L. I. Fatkhutdinova, O. O. Peltek, A. R. Muslimov, O. Y. Koval, I. E. Eliseev, A. Manchev, D. Gorin, I. I. Shishkin, R. E. Noskov, A. S. Timin, P. Ginzburg and M. V. Zyuzin, Controllable Synthesis of Calcium Carbonate with Different Geometry: Comprehensive Analysis of Particle Formation, Cellular Uptake, and Biocompatibility, *ACS Sustainable Chem. Eng.*, 2019, **7**(23), 19142–19156, DOI: **10.1021/acssuschemeng.9b05128**.

34 N. Lapshina, I. I. I. I. Shishkin, R. Nandi, R. E. R. E. Noskov, H. Barhom, S. Joseph, B. Apter, T. Ellenbogen, A. Natan, P. Ginzburg, N. Amdursky and G. Rosenman, Bioinspired Amyloid Nanodots with Visible Fluorescence, *Adv. Opt. Mater.*, 2019, **7**(5), 1–7, DOI: **10.1002/adom.201801400**.

35 H. Barhum, T. Alon, M. Attrash, A. Machnev, I. Shishkin and P. Ginzburg, Multicolor Phenylenediamine Carbon Dots for Metal-Ion Detection with Picomolar Sensitivity, *ACS Applied Nano Materials*, 2021, **4**(9), 9919–9931, DOI: **10.1021/acsanm.1c02496**.

36 J. Vandevondele, M. Krack, F. Mohamed, M. Parrinello, T. Chassaing and J. Hutter, Quickstep: Fast and Accurate Density Functional Calculations Using a Mixed Gaussian and Plane Waves Approach, *Comput. Phys. Commun.*, 2005, **167**(2), 103–128, DOI: **10.1016/j.cpc.2004.12.014**.

37 K. Momma and F. Izumi, VESTA 3 for Three-Dimensional Visualization of Crystal, Volumetric and Morphology Data, *J. Appl. Crystallogr.*, 2011, **44**(6), 1272–1276, DOI: **10.1107/S0021889811038970**.

38 J. VandeVondele and J. Hutter, Gaussian Basis Sets for Accurate Calculations on Molecular Systems in Gas and Condensed Phases, *J. Chem. Phys.*, 2007, **127**(11), 1–10, DOI: **10.1063/1.2770708**.

39 B. Miehlich, A. Savin, H. Stoll and H. Preuss, Results Obtained with the Correlation Energy Density Functionals of Becke and Lee, Yang and Parr, *Chem. Phys. Lett.*, 1989, **157**(3), 200–206, DOI: **10.1016/0009-2614(89)87234-3**.

40 P. J. Stephens, F. J. Devlin, C. F. Chabalowski and M. J. Frisch, Ab Initio Calculation of Vibrational Absorption and Circular Dichroism Spectra Using Density Functional Force Fields, *J. Phys. Chem.*, 1994, **98**(45), 11623–11627, DOI: **10.1021/j100096a001**.

41 A. Machnev, D. Ofer, I. Shishkin, V. Kozlov, C. Diaferia, A. Accardo, G. Morelli, B. Apter, A. Inberg, G. Rosenman and P. Ginzburg, Amplified Spontaneous Emission and Gain in Highly Concentrated Rhodamine-Doped Peptide Derivative, *Sci. Rep.*, 2021, **11**(1), 1–10, DOI: **10.1038/s41598-021-96982-5**.

42 S. Yamamoto and K. Tanaka, Molecular Size Effect on Curing Process for Epoxy and Amine Mixture, *Nihon Reoroji Gakkaishi*, 2021, **49**(2), 55–60, DOI: **10.1678/rheology.49.55**.

43 O. Belhadj, D. Hammiche, A. Boukerrou, J. F. Gérard and J. Duchet, Effect of Alfa Fiber Loading on the Mechanical, Physical and Dielectric Properties of Epoxy-Amine Composite, *J. Compos. Mater.*, 2022, **56**(23), 3563–3573, DOI: **10.1177/00219983221119269**.

44 A. Cuvellier, A. Torre-Muruzabal, N. Kizildag, L. Daelemans, Y. Ba, K. De Clerck and H. Rahier, Coaxial Electrospinning of Epoxy and Amine Monomers in a Pullulan Shell for Self-Healing Nanovascular Systems, *Polym. Test.*, 2018, **69**, 146–156, DOI: **10.1016/j.polymertesting.2018.05.023**.

45 S. Morsch, C. R. Wand, S. Gibbon, M. Irwin, F. Siperstein and S. Lyon, The Effect of Cross-Linker Structure on Interfacial Interactions, Polymer Dynamics and Network Composition in an Epoxy-Amine Resin, *Appl. Surf. Sci.*, 2023, **609**, DOI: **10.1016/j.apsusc.2022.155380**.

46 M. Puyadena, I. Calafel, E. G. de San Román, L. Martin, A. González and L. Irusta, Recyclable Epoxy Resin via Simultaneous Dual Permanent/Reversible Crosslinking Based on Diels–Alder Chemistry, *Macromol. Chem. Phys.*, 2021, **222**(17), DOI: **10.1002/macp.202100146**.

47 S. D. Pandita, L. Wang, R. S. Mahendran, V. R. MacHavaram, M. S. Irfan, D. Harris and G. F. Fernando, Simultaneous DSC-FTIR Spectroscopy: Comparison of Crosslinking Kinetics of an Epoxy/Amine Resin System, *Thermochim. Acta*, 2012, **543**, 9–17, DOI: **10.1016/j.tca.2012.04.024**.

This journal is © The Royal Society of Chemistry 2023